Three-dimensional structure of human RNase 1ΔN7 at 1.9 Å resolution

Joan Pous,[a]† Goretti Mallorquí-Fernández,[a,b]† Rosa Peracaula,[b] Simon S. Terzyan,[a]‡ Junichiro Futami,[c] Hiroko Tada,[c] Hidenori Yamada,[c] Masaharu Seno,[c] Rafael de Llorens,[b] F. Xavier Gomis-Rüth[a]* and Miquel Coll[a]

[a]Institut de Biologia Molecular de Barcelona, CID–CSIC, Jordi Girona 18–26, 08034 Barcelona, Spain, [b]Unitat de Bioquímica i Biologia Molecular, Departament de Biologia, Universitat de Girona, 17071 Girona, Spain, and [c]Department of Bioscience and Biotechnology, Faculty of Engineering, Okayama University, Tsushima-Naka, Okayama 700-8530, Japan

† These authors contributed equally to this work and share first authorship.
‡ Present address: Crystallography Department, OMRF, 825 NE 13th Street, Oklahoma City, OK 73104, USA.

Correspondence e-mail: xgrcvi@ibmb.csic.es

Human pancreatic ribonuclease 1 (RNase 1) is considered to be the human counterpart of bovine pancreatic RNase A. Truncation of seven amino-acid residues from the amino-terminal sequence resulted in RNase 1ΔN7, which has a reduced ribonucleolytic activity and a lower affinity for the human placental RNase inhibitor (PRI). This RNase 1 variant has been cloned, heterologously overexpressed, purified and crystallized. Its crystal structure has been determined and refined using data to 1.9 Å resolution. The molecule displays the $\alpha + \beta$ folding topology typical of members of the RNase A superfamily. The main distinct features found in RNase 1ΔN7 are basically located in three loops affecting the fitting of the enzyme to the active site of subtilisin and the shape of the B2 subsite. These changes, taken with the lack of the catalytically active residue Lys7, may explain the reduced affinity of RNase 1ΔN7 for PRI and the low ribonucleolytic activity of the protein when compared with the native enzyme.

1. Introduction

Interest in human ribonucleases (RNases) has increased in recent years as a result of major knowledge of their biological properties and possible therapeutic applications (Schein, 1997; Rybak & Newton, 1999). To date, six different genes have been described in humans (Rosenberg & Dyer, 1996). Some of these human ribonucleases, namely angiogenin, eosinophil-derived neurotoxin (EDN) and eosinophil cationic protein (ECP), are involved in important biological functions such as angiogenic activity (Strydom et al., 1985), neurotoxicity (Durack et al., 1981) and cytotoxicity (Domachowske et al., 1998), respectively. Ribonucleolytic activity was not always found to be a condition for these special activities (Rosenberg, 1998; Strydom, 1998). The biological role of the other human ribonucleases, RNase 1, RNase 4 and RNase 6, remains still to be unveiled.

In addition to these discoveries, important progress in the structural field has also been achieved. Several structures of human RNases have been solved by X-ray diffraction: angiogenin (Acharya et al., 1994), EDN (Mosimann et al., 1996), RNase 4 (Terzyan et al., 1999) and ECP (Boix et al., 1999; Mallorquí-Fernández et al., 2000). The data reported show that all these enzymes display a global topological similarity to the archetypal bovine RNase A, as they all belong to the same class of mammalian hydrolases. Some differences have been found, however, in the residues shaping the ribonucleolytic active site, which accounts for their distinct specific activities and substrate preferences. Additional structural differences have also been found in some external loops and in

the surface charge distribution, which could be related to their distinct biological activities (Acharya *et al.*, 1994; Mosimann *et al.*, 1996; Terzyan *et al.*, 1999; Boix *et al.*, 1999; Mallorquí-Fernández *et al.*, 2000).

The object of the presently reported investigations, ribonuclease 1 (RNase 1), is the human homologue of bovine pancreatic RNase A (70% of identity), one of the most exhaustively studied enzymes (D'Alessio & Riordan, 1997) (Fig. 1). Both proteins display similar enzymatic properties (Sorrentino & Libonati, 1997), as the amino-acid residues involved in the catalytic subsites are conserved. However, some differences are found in their activity towards double-stranded RNA. RNase 1 has a higher activity than RNase A (two orders of magnitude), which is probably attributable to the replacement of neutral residues in the latter by basic amino acids in the former. It has been postulated that strong local positive electrostatic potentials could destabilize the double strand (Sorrentino & Libonati, 1997).

As mentioned before, the biological function of human RNase 1 is still unknown. While RNase A degrades bacterial RNA from the diet in ruminants, the function of the homologous enzymes in other mammals is not clear. RNase A is present only in bovine pancreas. In bovine brain, for instance, another type of ribonuclease is found (Sasso *et al.*, 1999). In contrast, human RNase 1 has been found in most human body tissues, being mainly expressed in the pancreas (Futami *et al.*, 1997; Fernández-Salas *et al.*, 2000), suggesting a general role for this enzyme. Other differences are found in the glycosylation pattern of both proteins. While RNase A is little glycosylated, with only one N-glycosylation site (Asn34; Beintema, 1986; see Fig. 1), RNase 1 has three potential glycosylation sites (Asn34, Asn76 and Asn88), with different degrees of glycosylation depending on its tissue of origin (Yamashita *et al.*, 1986; Beintema *et al.*, 1988; Ribó *et al.*, 1994).

Most interestingly, distinct glycosylation patterns have been detected in human RNase 1 produced by normal pancreas and in RNase 1 produced by human pancreatic tumour cells (Fernández-Salas *et al.*, 2000). Therefore, RNase 1 can be considered as a marker that could permit early detection of pancreatic tumours.

The objective of the present work was to determine the structure of human RNase 1. The data obtained will allow us to elucidate the most significant differences from the structure of bovine RNase A. RNase 1 has a C-terminal extension of four amino acids (see Fig. 1), which is only present in non-ruminant mammals. These amino acids are not essential for ribonuclease activity, but removing them enhances the enzymatic activity (Bal & Batra, 1997). The N-terminal region is important in RNase A homologues, as it plays an important role in their catalytic activity, ribonuclease–inhibitor interaction and cytotoxicity (Boix *et al.*, 1996).

Several crystallization trials were carried out with recombinant full-length RNase 1, but none succeeded in rendering diffraction-quality crystals. Because RNase 1 is so similar to RNase A, which crystallizes easily (Gilliland, 1997), we wondered which features could account for this different behaviour. One possible reason could be found in the highly positive N-terminus of RNase 1. Of residues 3–13 of the N-terminus part which forms an α-helix in RNase A, two residues, Lys7 and Arg10, are basic in RNase 1, as is Lys1 (RNase A numbering, see Fig. 1). In RNase 1, however, two more residues, Arg4 and Lys6, are also basic. We stated the possibility that this highly positive charge density could prevent crystal formation. These observations lead us to produce a protein variant lacking some of these first amino-acid residues.

Truncation of seven amino-acid residues at the amino-terminal sequence results in an enzyme (RNase 1ΔN7) with reduced ribonucleolytic activity (approximately nine times lower than RNase 1 towards yeast RNA), probably owing to the lack of Lys7, which is putatively involved in p$_2$ subsite shaping. The CD spectrum of this protein indicates a folding similar to native RNase 1 (Futami *et al.*, 1995). The N-terminal region is also important for binding of RNase A homologues to ribonuclease inhibitor (RI); in particular, Lys7 and Gln11 in RNase A contribute to the interaction with the inhibitor by forming hydrogen bonds with Ser456 of porcine RI (Kobe & Deisenhofer, 1995). Accordingly, RNase 1ΔN7 showed a reduced binding ability to PRI (Futami *et al.*, 1995), which makes it a good candidate for a cytotoxic ribonuclease. When

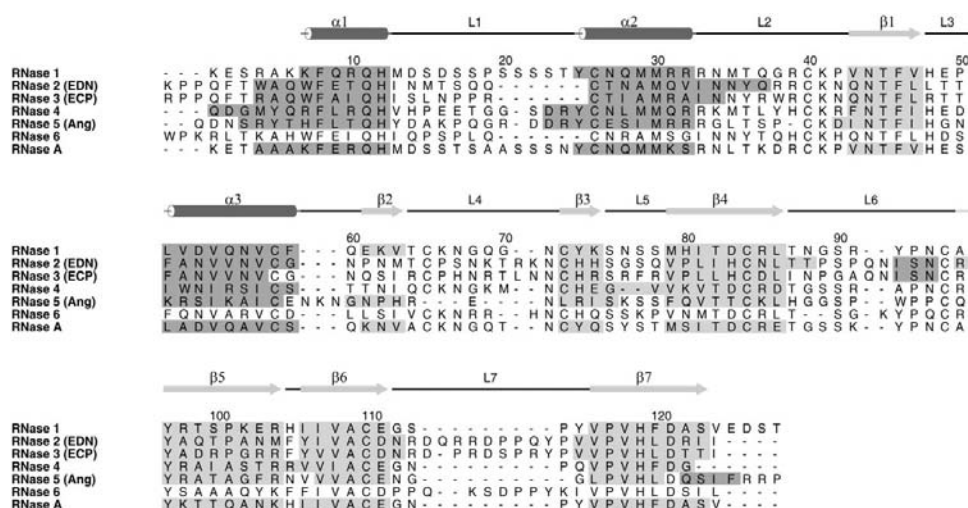**Figure 1**
Alignment of the amino-acid sequences of human RNases and bovine pancreatic RNase A. The α-helices and β-strand of RNase 1ΔN7 are displayed as labelled dark rods and light arrows, respectively. The topologically equivalent secondary-structure elements in the enzymes with known three-dimensional structures are shaded: α-helices with a dark grey background and β-strands with a light grey background. The numbering corresponds to both RNase 1 and RNase A.

comparing the effect on cell growth of the fused proteins human RNase1-bFGF (basic fibroblast growth factor) and RNase 1ΔN7-bFGF in melanoma cells B16/BL6, the inhibitory effect of both fused proteins was similar, being slightly higher for the RNase 1ΔN7 fused protein (Futami *et al.*, 1999). Similar behaviour of RNase 1ΔN7-EGF (epidermal growth factor) was observed against tumour cells overexpressing EGF receptors (Watanabe *et al.*, 1999). The difference in cytotoxicity between the RNase 1ΔN7 and RNase 1 fused proteins was not as high as expected, probably because of the lower ribonuclease activity of RNase 1ΔN7 and its unstable character in solution owing to the truncation of the N-terminal part of the protein.

In this paper, we report the crystal structure of human RNase 1ΔN7 at 1.9 Å resolution and a detailed comparison with its bovine homologue RNase A. The role of the missing N-terminal region in RI binding is further discussed based on this comparison. This new structure, corresponding to a molecule that could be used as a potential marker for pancreatic tumours, establishes the structural fundamentals for early diagnosis of this pathology.

2. Materials and methods

2.1. Protein preparation

Recombinant human RNase 1ΔN7 was purified from *Escherichia coli* as described previously (Futami *et al.*, 1995). Briefly, plasmid pBO54 containing human RNase 1 cDNA encoding a protein N-terminally truncated by seven amino-acid residues was cloned downstream of the T7 promoter and used to transform *E. coli* BL21 (DE3) cells harbouring the plasmid pLysS. The transformant was cultured in LB broth and the expression of recombinant protein was induced by 0.4 mM of isopropyl 1-thio-β-D-galactopyranoside with continued cultivation for a further 3 h. Since the recombinant human RNase 1ΔN7 was produced as inclusion bodies, the protein was disolved in 8 M urea under reducing conditions and refolded in redox buffer. The refolded protein was further purified by cation-exchange and reverse-phase column chromatography. The recovery of the recombinant protein was 1.1 mg from 1 l culture. The purified recombinant human RNase 1ΔN7 was assessed for amino-acid composition and amino-terminal sequence, which were consistent with the design of the construct. Human RNase 1ΔN7 has an extra alanine at the amino terminus that, unlike the first methionine, has not been removed during expression in *E. coli*. However, the alanine does not correspond to the native residue of RNase 1 at the same position.

2.2. Treatment of RNases with subtilisin

Solutions of 0.5 mg ml^{-1} of RNase A or RNase 1 in 0.1 M Tris–HCl, 0.1 M NaCl pH 8 were treated with 1–10%(w/w) subtilisin (subtilopeptidase A from *Bacillus subtilis*; Sigma) either at room temperature or 277 K as described previously (Richards & Wyckoff, 1971). The reactions were stopped by addition of 2 M HCl, 0.2 M acetic acid. The enzymatic reactions were followed by either SDS–PAGE or zymogram (Bravo *et al.*, 1994).

2.3. Crystallization and data collection

Crystals were grown by the vapour-diffusion method at room temperature from hanging drops containing 1 µl of 20 mg ml^{-1} of freeze-dried protein in pure water and 1 µl of precipitant solution containing 7%(v/v) polyethylene glycol 8K and 0.1 M Tris–HCl at pH 8.5 equilibrated against 1 ml of precipitant solution. These crystals have a laminar shape with typical dimensions of 0.30 × 0.25 × 0.05 mm. A close inspection of the crystals showed that they were actually plate clusters. To obtain single crystals, the clusters were broken into pieces by pressing along the interface. These crystals were cryocooled at 110 K (using 15% PEG 8K, 15% ethylene glycol as a cryoprotectant) and data collection was performed at ESRF beamline ID14-EH2 using a Quantum CCD area detector.

Prior to data collection, a fast annealing and refreezing of the crystals by interrupting the Cryostream increased the quality of the data considerably by eliminating solvent rings. A

Table 1
Data-collection, processing and refinement statistics for RNase 1ΔN7.

Values in parentheses correspond to the highest resolution shell (2.0–1.9 Å).

Data statistics	
Space group	$P2_12_12_1$
Unit-cell dimensions (Å)	a = 32.8, b = 42.6, c = 80.0
Resolution (Å)	19.90–1.90
Completeness (%)	92.9 (87.2)
$\langle I \rangle / \langle \sigma_I \rangle$	4.4 (2.0)
Average multiplicity	3.2 (3.1)
No. of observed reflections	27390
No. of unique reflections	8618
R_{merge}† (%)	11.3 (36.4)
Refinement statistics	
No. of molecules per asymmetric unit	1
Resolution range used for refinement (Å)	19.90–1.90
No. of reflections in working set	8143
No. of reflections in test set	449
Completeness (%)	92.3
No. of protein atoms included in refinement	948
No. of solvent molecules	137
R factor/R_{free}‡	0.196/0.251
R.m.s. deviations from target values	
Bond lengths (Å)	0.007
Bond angles (°)	1.61
Average B factors (Å^2)	
Protein, overall	22.1
Main chain	20.9
Side chain	23.3
Water	33.1
Ramachandran statistics	
Most favoured regions (%)	83.8
Additional allowed regions (%)	13.3
Generously allowed regions (%)	2.9
Disallowed regions (%)	0.0

† $R_{merge} = \sum |I_h - \langle I_h \rangle| / \sum \langle I_h \rangle$ where $\langle I_h \rangle$ is the average intensity of reflection h and symmetry-related reflections. ‡ $R = R_{free} = \sum ||F_o| - |F_c|| / \sum |F_o|$ calculated for the reflections of the working and test (5%) sets, respectively.

total of 100 frames was collected at a wavelength of 0.933 Å. The distance between the crystal and the detector was 130 mm and the oscillation angle was 1°.

The crystals belong to space group $P2_12_12_1$, with unit-cell parameters a = 32.8, b = 42.6, c = 80.0 Å. The value of the Matthews parameter suggested the presence of one monomer per asymmetric unit (V_M = 1.9 Å^3 Da^{-1}; Matthews, 1968). Data were processed with *MOSFLM* (Leslie, 1991) and *SCALA* (Evans, 1993). Data-processing statistics are presented in Table 1.

2.4. Structure solution, model building and refinement

The structure of the enzyme was solved by molecular replacement with the *AMoRe* package (Navaza, 1994), using bovine RNase A (Wlodawer, 1988; PDB code 7rsa) modified and truncated in accordance with the amino-acid sequence of RNase 1ΔN7 as a search model. Rotation and translation functions were calculated using data in the 15–3.0 Å resolution range. A clear solution was obtained that, after rigid-body refinement, displayed a correlation coefficient of 49.7% (second highest solution 32.7%) and an R factor of 44.4% (second solution 51.9%).

The structure refinement was carried out with *CNS* v.1.0 (Brunger *et al.*, 1998) using all data in the 20–1.9 Å resolution range. Initial calculated σ_A-weighted $F_o - F_c$ and $2F_o - F_c$ maps inspected on a Silicon Graphics workstation using *TURBO-FRODO* (Roussel & Cambillau, 1989) showed a different path than the model for amino acids 17–22 of loop L1 (see Figs. 3a and 3b) and weak density for loop L4 and residues 89–91 of loop L6. The building of L1 was performed manually, as its trajectory was clearly visible in the maps. The final building of the last two conflicting loops (L4 and L6) was carried out by omitting the corresponding residues and applying one cycle of torsion-angle-restrained simulated annealing followed by a calculation of σ_A-weighted $F_o - F_c$ maps. Clear electron density for L4 showed a different conformation of this exposed loop to that in RNase A (Figs. 3c and 3d). Cycles of positional refinement and temperature-factor refinement were alternated with manual model building. In the last steps of refinement, solvent molecules were placed at stereochemically reasonable positions if they displayed density in both $2F_o - F_c$ (1σ) and $F_o - F_c$ (2.5σ) maps. Two alternative conformations were also modelled for residues Arg31, Lys41, Ser79 and Leu86. The final model of RNase 1ΔN7 contains all the residues of the chemical sequence of RNase 1ΔN7 except the last three C-terminal residues Asp126, Ser127 and Thr128 and 137 water molecules. Table 1 summarizes the refinement and quality of the final model.

Least-squares superposition of RNase 1ΔN7 with RNase A, EDN, ECP, RNase 4 and angiogenin was performed with *TURBO-FRODO* (Roussel & Cambillau, 1989). Figures were constructed with *Bobscript* v2.4 (Esnouf, 1997) and *TURBO-FRODO*. The sequence-alignment figure was produced with *Alscript* (Barton, 1993).

3. Results and discussion

3.1. Overall structure

RNase 1ΔN7 displays an (α + β) type polypeptide chain folding, with approximate molecular dimensions of 30 × 40 × 40 Å and a V shape with the active-site cleft in the middle (Fig. 2a). It encompasses three α-helices (α1–α3) in the N-terminal part and seven β-strands (β1–β7), the first between helices α2 and α3 and the others after helix α3 (Fig. 2a). It also shows a 3_{10} helix from Val57 to Gln60. The β-strands β3 + β4 and β5 + β6 extend from one end of the structure to the other in an antiparallel manner, forming the overall V shape, with β-strands β1 and β7 appended to them from either side. Helix α2 is packed against the central sheet on the opposite face of the cleft and, in combination with helix α3, delimits the active-site cleft on one side.

The secondary-structural elements are connected by seven loops (L1–L7) comprising about 30% of the protein residues. The structure is stabilized by four disulfide bridges: Cys26–Cys84 bridges helix α2 and strand β4, Cys40–Cys95 connects loops L2 and L6, Cys58–Cys110 links α3 and strand β6 and Cys65–Cys72 joins loop L4 and β3.

The disulfide-bridge pattern and the overall structure closely resemble those of RNase A (Wlodawer *et al.*, 1988), ECP (Boix *et al.*, 1999; Mallorquí-Fernández *et al.*, 2000), EDN (Mosimann *et al.*, 1996), RNase 4 (Terzyan *et al.*, 1999) and angiogenin (Acharya *et al.*, 1994).

3.2. Comparison of RNase 1ΔN7 with EDN, ECP, RNase 4 and angiogenin

RNase 1ΔN7 displays the fold common to all RNases described [RNase 2 alias EDN (Mosimann *et al.*, 1996), RNase 3 alias ECP (Boix *et al.*, 1999; Mallorquí-Fernández *et al.*, 2000; PDB code 1dyt), RNase 4 (Terzyan *et al.*, 1999; PDB code 1rnf), angiogenin (Acharya *et al.*, 1994; PDB code 1ang), RNase A (Wlodawer *et al.*, 1988; PDB code 7rsa)]. The least-squares superposition of their structures, represented in Fig. 2(b), shows that the secondary-structure elements mostly coincide, while some non-regular elements, mainly the loops, greatly diverge (secondary-structure elements in all compared structures as defined by *PROCHECK*; Laskowski *et al.*, 1993; see Fig. 1).

In RNase 1ΔN7, helix α1 starts at residue Phe8 and ends at residue His12. Although the beginning of this helix is still unknown for the full form of RNase 1, it finishes at His12 at its C-terminal end, as do the corresponding helices of the other human RNases and RNase A (see Fig. 1).

When comparing helices α2, that of EDN is the longest and contains 12 residues compared with ten in RNase 4 and angiogenin, nine in ECP and eight in RNase 1ΔN7 and RNase A. Compared with RNase 1ΔN7 and RNase A, in RNase 4 and angiogenin this helix is extended towards the N-terminus of the polypeptide chain, while in EDN and ECP it is elongated in the opposite direction. In RNase 1ΔN7, as in RNase A and RNase 4, the last three residues of helix α3 correspond to a 3_{10} helix; the helix is one residue longer than α3 of angiogenin and two residues longer than α3 of ECP.

The β-sheet of RNase 1ΔN7 has two split strands (β3 + β4) and (β5 + β6), in a similar manner to EDN [(β2 + β3) and (β4 + β5)], ECP [(β2 + β3) and (β4 + β5)], angiogenin [(β3 + β4) and (β5 + β6)] and RNase A [(β3 + β4) and (β5 + β6)]. RNase 4 is the only member of the family that shows a continuous strand β5 (Terzyan *et al.*, 1999). The short strand β2 of angiogenin and RNase A is also present in the structure of RNase 1ΔN7.

Among the segments displaying major differences in the six analysed structures is the loop connecting helices α1 and α2 (L1 in RNase 1ΔN7), which is of diverging length (seven residues in ECP and EDN, nine residues in RNase 4 and angiogenin, ten in RNase 1ΔN7 and 12 in RNase A). The loop that links strands β4 and β5 (L6) of ten residues (Thr87–Ala96) has a different conformation in the presently described structure when compared with the other human RNases. The conformation of the loop connecting helix α2 with strand β1 (L2) is very similar in all structures except for EDN because of its elongated helix α2, as mentioned above.
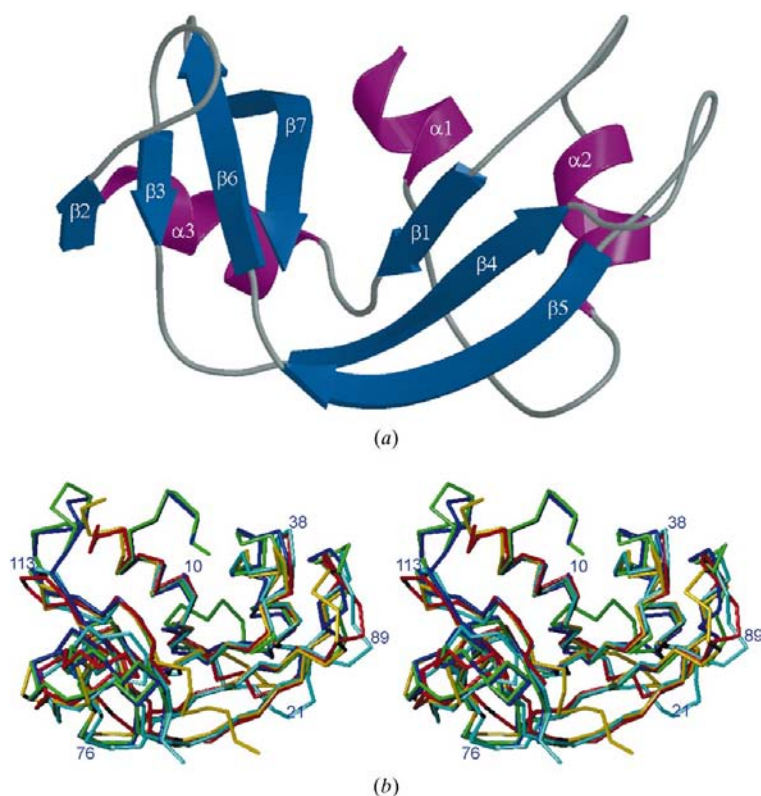
3.3. Overall comparison of RNase 1ΔN7 with bovine RNase A

RNase A and RNase 1 are both secretory-type ribonucleases that display 70% sequence similarity and present comparable ribonuclease activity (Sorrentino & Libonati,
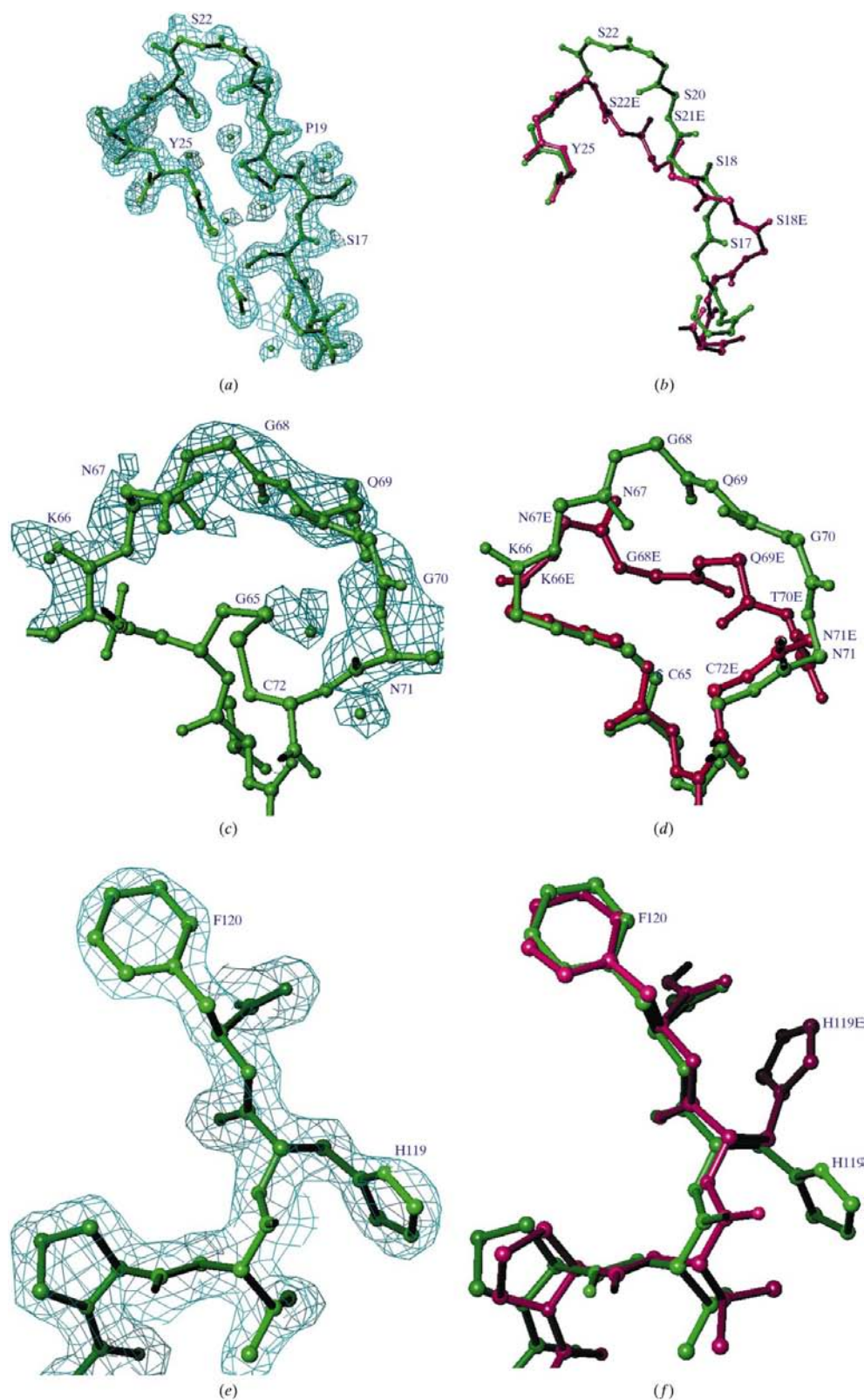

(a)

(b)

Figure 2
(*a*) Ribbon representation of the RNase 1ΔN7 polypeptide fold. The labelled helices (α1–α3), strands (β1–β6) and loops are shown as helical ribbons, arrows and thin tubes, respectively. Labelling is according to Fig. 1. (*b*) Superimposed RNase C$^\alpha$ structures. The displayed traces correspond to RNase 1ΔN7 (cyan blue), human ECP (blue; PDB code 1dyt), EDN (green), RNase 4 (red; PDB code 1rnf) and angiogenin (yellow; PDB code 1ang). Some RNase 1ΔN7 residues are labelled.

1997). However, the comparison of the crystal structures of RNase A (Wlodaver *et al.*, 1988) with RNase 1ΔN7 reveals some differences in their three-dimensional structures. The r.m.s. deviation of the C$^\alpha$ atoms after superposition is 1.08 Å. Despite this close topological similarity, different conformations are found in two loops (16–23 and 66–70), with major variations of up to 6 Å between the main-chain atoms of topologically equivalent residues.

Loop 16–23 contains the subtilisin cleavage site for RNase A, between residues Ala20 and Ser21, that produces the enzymatically active RNase S, which comprises of the S-peptide (residues 1–20) bound to the S-protein (residues 21–124) (Richards & Wyckoff, 1971). Treatment of RNase 1 with subtilisin under similar conditions does not transform RNase 1 into an S-protein and an S-peptide. This distinct behaviour of RNase 1 towards subtilisin is also observed for other ribonucleases such as rat pancreatic ribonuclease (Gupta *et al.*, 1999) and angiogenin (Harper & Vallee, 1998). The amino-acid sequence and the backbone in this region, residues 15–25, is quite variable in these ribonucleases and, as with RNase 1ΔN7, is quite distinct from RNase A. The main chain in RNase 1ΔN7 follows a markedly different course from RNase A (Figs. 3*a* and 3*b*). This divergence begins at residue Asn16 in RNase 1ΔN7 (RNase A has a serine at this position) and a displacement of one residue is observed between both proteins (RNase 1ΔN7 and RNase A), with a divergence of 4.5 Å between residues Ser17 (RNase 1ΔN7) and Ser18 (RNase A). The main chain joins two residues upstream (18 and 19, RNase 1ΔN7 numbering) and deviates again later between Ser21 (RNase 1ΔN7) and Ser22 (RNase A), with a maximum divergence of 6.2 Å. From Ser23 onwards both main chains are superimposable. These differences may account for the different behaviour of both enzymes towards subtilisin. Molecular docking of this region of RNase 1ΔN7 in the active site of subtilisin shows steric incompatibility, as opposed o the fitting of RNase A (data not shown).

The backbone of loop L4 (residues 66–71) also shows a different conformation, probably as a consequence of the presence of two glycines at positions 68 and 70 as opposed to the one (Gly68) in RNase A (Figs. 3*c* and 3*d*). This loop is found between two cysteines (Cys65 and Cys72) that form a disulfide bridge which is conserved in most of the members of the RNase superfamily, with the exceptions of angiogenin and frog RNases (Youle & D'Alessio, 1997). While the residues before Cys65 and after Cys72 are part of the rigid backbone of the molecule, the loop residues are very flexible. The orientations of the side chains of Lys66, Asn67 and Gln69 are not well defined by electron density, reflecting this inherent mobility. This conformational change was unexpected as both Asn71 O$^\delta$ and Gln69 O$^\varepsilon$ play a key role in the active site of RNase A by hydrogen bonding a substrate adenine at the B$_2$ subsite (Fontecilla-Camps *et al.*, 1994; see below). In

Figure 3
Close view of the RNase 1ΔN7 loop L1, loop L4 and His119. (*a*) The final model, including side chains and the corresponding $2F_o - F_c$ calculated map for the loop L1 at $\sigma = 1$, is shown. (*b*) Superimposed RNase 1ΔN7 (green) and RNase A (dark pink) backbone structures. Some residues of both proteins are labelled. (*c*) The final model, including side chains and the corresponding $F_o - F_c$ omit map (cyan blue), for the loop L4 at $\sigma = 2.5$ is shown. (*d*) Superimposed RNase 1ΔN7 (green) and RNase A (dark pink) backbone structures of the same region. Some residues of both proteins are labelled. (*e*) The final model and the corresponding $2F_o - F_c$ calculated map around His119 at $\sigma = 1$ is shown. (*f*) Superimposed RNase 1ΔN7 (green) and RNase A (dark pink) structures.

RNase 1ΔN7 these residues seem to adopt conformations that differ substantially from those of RNase A and their side chains are not directed towards the active site of the enzyme. The well defined side chain of Asn71 is surface-exposed in contrast to that of RNase A. However, the varying conformation observed in this loop would allow the carbonyl O atom of Gln69 to be sufficiently close to the B_2 subsite to play a similar role to that of Gln69 O^{ε} in the RNase A–d(ApTpA-pApG) complex (Fontecilla-Camps *et al.*, 1994). This markedly changed loop in RNase 1ΔN7 may be related to the low ribonuclease activity of RNase 1ΔN7 towards dinucleotides such as CpA (discussed below).

3.4. Comparison of the active-site architecture

The active-site cleft in RNase A is formed by several subsites that are responsible for binding of bases (B), riboses (R) and phosphates (p) of a substrate. The phosphate group of the phosphodiester bond hydrolysed by the enzyme binds to p_1. B_1 is specific for pyrimidines and B_2 shows a preference for purines. The catalytic site corresponds to R_1p_1; the other phosphate non-catalytic subsites at the 5′ side of the scissile phosphodiester bond in p_1 are named, in consecutive order, p_0 and p_{-1}, while p_2 is the corresponding binding subsite on the 3′ side of p_1 (Parés *et al.*, 1991).

In RNase 1ΔN7 all the corresponding residues of the active site are present except for Lys7. The main residues of the catalytic site (Gln11, His12, Lys41 and His119) occupy similar positions, except for the arrangement of His119, which adopts the inactive conformation shown in the complex between RNase A and 3′-CMP

(Zegers *et al.*, 1994; Figs. 3*e* and 3*f*). In the interaction between the nucleotide and the enzyme in its active form, His119 $N^{\delta 1}$ establishes one hydrogen bond with the O5' of the ribose ring at R_2 and participates in the catalysis (Fontecilla-Camps *et al.*, 1994). His119 in RNase 1ΔN7 could easily adopt the active conformation by a rotation of the χ_1 and χ_2 torsion angles in order to interact with the O5' of the ribose at R_2 adjacent to the scissile bond and participate in the catalysis in a similar manner as in the RNase A–d(ApTpApApG) complex (Fontecilla-Camps *et al.*, 1994). The p_2 subsite is altered owing to the lack of Lys7, which is responsible for binding the phosphate group at p_2 in the RNase A–d(ApTpApApG) complex (Fontecilla-Camps *et al.*, 1994). The B_2 subsite is also altered owing to the different conformation of the protein in the loop that contains Gln69 and Asn71. Thus, the interaction of the side chains of Gln69 and Asn71 with the adenine base at this subsite seems not to be possible in RNase 1ΔN7 (see above). These significant changes found in subsites p_2 and B_2 of RNase 1ΔN7 may explain the low activity of this enzyme in comparison to RNase A and native RNase 1. Proportionally, RNase 1ΔN7 is much less active towards CpA (24 times lower than RNase 1) than towards yeast RNA (nine times lower than RNase 1) (Futami *et al.*, 1995), suggesting that the different shape of the B_2 subsite may be responsible for this lower activity towards a dinucleotide that contains an adenine base.

3.5. Comparison of RNase 1ΔN7 with the complex of ribonuclease inhibitor and bovine RNase A

RNase 1ΔN7 shows a lower affinity for human placental inhibitor (PRI), which may account for its major cytotoxicity in comparison to other ribonucleases (Futami *et al.*, 1999; Watanabe *et al.*, 1999). RNase 1ΔN7 requires three times as much PRI to observe 50% inhibition towards yeast RNA compared with RNase 1. In order to investigate which residues may be responsible for the low affinity of the enzyme for the inhibitor, we have superimposed RNase 1ΔN7 structure with those of the complexes bovine RNase A–porcine ribonuclease inhibitor (Kobe & Deisenhofer, 1995) and angiogenin–human ribonuclease inhibitor (Papageorgiou *et al.*, 1997).

In both complexed structures, PRI binds to RNases in a similar way by docking into the active site and establishing contacts with several active-site residues, thus inhibiting their enzymatic activity by sterically impeding the access of substrates. However, both complex structures showed differences in the inhibitor residues that contact active-site residues or other loop residues responsible for binding. The interaction between the ribonuclease inhibitor and the distinct members of the ribonuclease superfamily reveals a high flexibility of some of the inhibitor regions in order to bind each member of the family with high affinity.

The superposition of RNase 1ΔN7 with RNase A in its complex with porcine ribonuclease inhibitor (Kobe & Deisenhofer, 1995) gives an r.m.s.d. of 0.37 Å. One of the residues that contributes most to the binding energy in the PRI–RNase A complex is Lys7, absent in RNase 1ΔN7, which contacts Ser456 of the inhibitor. This interaction seems impossible wtih RNase 1ΔN7, as no residue of the molecule is close enough to contact Ser456. Therefore, the lack of Lys7 is probably responsible for the low affinity of RNase 1ΔN7 for PRI. In angiogenin–PRI, a similar contact is established by His8 of Ang and the homologous Ser460 of PRI. However, in this case the interaction is not as strong as with RNase A. On the other hand, loop L4 (residues 66–71), involved in the binding of RNase A to PRI (region Cys404–Tyr433), has a different conformation in RNase 1ΔN7. Most of the amino acids in loop L4 cannot establish the same contacts with the inhibitor. However, the flexibility of this loop could allow adaptation to the inhibitor area and thus it cannot be so relevant in explaining the low affinity of RNase 1ΔN7.

Other areas of interest such as loop L6 (residues 88–91), loop L2 (residues 34–39) or the amino acids of the active site of RNase 1ΔN7 do not differ significantly from the homologous residues in RNase A and could probably establish similar interactions with the inhibitor.

4. Conclusions

The determination of the crystal structure of RNase 1ΔN7 gives us a better picture of human RNases. The overall shape of these proteins closely resembles that of the archetypal bovine RNase A (Fig. 2*b*). It could be inferred that the most divergent regions in this superfamily of enzymes, mainly loops L1 (residues 15–25) and L6 (residues 88–95) (RNase A numbering), may be responsible for other activities than the ribonucleolytic activity. Accordingly, the enzymatic cleavage of these enzymes by subtilisin is directly related to the conformation of the loop L1 fitting the active site of subtilisin. On the other hand, RNase 1ΔN7 shows a markedly different conformation of the backbone in loop 66–71 with respect to the other human RNases and RNase A. This is one of the factors that together with the lack of Lys7 accounts for the low ribonucleolytic activity of RNase 1ΔN7 towards dinucleotides such as CpA, owing to the change in the B_2 subsite of the enzyme.

RNase 1ΔN7 has a potential function as a cytotoxic RNase because of its low affinity for the ubiquitously expressed ribonuclease inhibitor. The lack of Lys7 allows RNase 1ΔN7 to exhibit ribonucleolytic activity and is probably mainly responsible for its reduced affinity for RI. The superposition of RNase 1ΔN7 with the complex RNase A–porcine ribonuclease inhibitor shows that the contact established by Lys7 in RNase A, which energetically favours the binding with the inhibitor, is not possible in the molecule. The features described above could contribute to improving the knowledge of RNase 1 and to new applications of RNase 1 in cancer diagnostics.

References

Acharya, K. R., Shapiro, R., Allen, S. C., Riordan, J. F. & Vallee, B. L. (1994). *Proc. Natl Acad. Sci. USA*, **91**, 2915–2919.

Bal, H. P. & Batra, J. K. (1997). *Eur. J. Biochem.* **245**, 465–469.

Barton, G. J. (1993). *Protein Eng.* **6**(1), 37–40.

Beintema, J. J. (1986). *J. Mol. Evol.* **24**, 118–120.

Beintema, J. J., Blank, A., Schieven, G. L., Dekker, C. A., Sorrentino, S. & Libonati, M. (1988). *Biochem. J.* **255**, 501–505.

Boix, E., Leonidas, D. D., Nikolovski, Z., Nogués, M. V., Cuchillo, C. M. & Acharya, K. R. (1999). *Biochemistry*, **38**, 16794–16801.

Boix, E., Wu, Y., Vasandani, V. M., Saxena, S. K., Ardelt, W., Ladner, J. & Youle, R. J. (1996). *J. Mol. Biol.* **257**, 992–1007.

Bravo, J., Fernández, E., Ribó, M., de Llorens, R. & Cuchillo, C. M. (1994). *Anal. Biochem.* **219**, 82–86.

Brunger, A. T., Adams, P. D., Clore, G. M., DeLano, W. L., Gros, P., Grosse-Kunstleve, R. W., Jiang, J. S., Kuszewski, J., Nilges, M., Pannu, N. S., Read, R. J., Rice, L. M., Simonson, T. & Warren, G. L. (1998). *Acta Cryst.* D**54**, 905–921.

D'Alessio, G. & Riordan, J. F. (1997). *Ribonucleases: Structures and Functions.* New York: Academic Press.

Domachowske, J. B., Dyer, K. D., Adams, A. G., Leto, T. L. & Rosenberg, H. F. (1998). *Nucleic Acids Res.* **26**, 3358–3363.

Durack, D. T., Ackerman, S. J., Loegering, D. A. & Gleich, G. J. (1981). *Proc. Natl Acad. Sci. USA*, **78**, 5165–5169.

Esnouf, R. M. (1997). *J. Mol. Graph.* **15**, 132–134.

Evans, P. R. (1993). *Proceedings of the CCP4 Study Weekend. Data Collection and Processing*, edited by L. Sawyer, N. Isaacs & S. Bailey, pp. 114–122. Warrington: Daresbury Laboratory.

Fernández-Salas, E., Peracaula, R., Frazier, M. L. & de Llorens, R. (2000). *Eur. J. Biochem.* **267**, 1484–1494.

Fontecilla-Camps, J. C., de Llorens, R., le Du, M. H. & Cuchillo, C. M. (1994). *J. Biol. Chem.* **269**, 21526–21531.

Futami, J., Seno, M., Kosaka, M., Tada, H., Seno, S. & Yamada, Y. (1995). *Biochem. Biophys. Res. Commun.* **216**, 406–413.

Futami, J., Seno, M., Ueda, M., Tada, H. & Yamada, H. (1999). *Protein Eng.* **12**, 1013–1019.

Futami, J., Tsushima, Y., Murato, Y., Tada, H., Sasaki, J., Seno, M. & Yamada, H. (1997). *DNA Cell Biol.* **16**, 413–419.

Gilliland, G. L. (1997). *Crystallographic Studies of Ribonuclease Complexes.* In *Ribonucleases: Structures and Functions*, edited by G. D'Alessio & J. F. Riordan. New York: Academic Press.

Gupta, V., Muylderman, S., Wyns, L. & Salunke, D. M. (1999). *Proteins*, **35**, 1–12.

Harper, J. W. & Vallee, B. L. (1998). *J. Protein Chem.* **7**, 355–63.

Kobe, B. & Deisenhofer, J. (1995). *Nature (London)*, **374**, 183–186.

Laskowski, R. A., MacArthur, M. W., Moss, D. S. & Thornton, J. M. (1993). *J. Appl. Cryst.* **26**, 283–291.

Leslie, A. (1991). *Crystallographic Computing V*, edited by D. Moras, A. D. Podjarny & J. C. Thierry, pp. 27–38. Oxford University Press.

Mallorquí-Fernández, G., Pous, J., Peracaula, R., Maeda, T., Tada, H., Yamada, H., Seno, M., de Llorens, R., Gomis-Rüth, F. X. & Coll, M. (2000). *J. Mol. Biol.* **300**, 1297–1310.

Matthews, B. W. (1968). *J. Mol. Biol.* **33**, 491–497.

Mosimann, S. C., Newton, D. L., Youle, R. J. & James, M. N. G. (1996). *J. Mol. Biol.* **260**, 540–552.

Navaza, J. (1994). *Acta Cryst.* A**50**, 157–163.

Papageorgiou, A. C., Shapiro, R. & Acharya, K. R. (1997). *EMBO J.* **16**, 5162–5177.

Parés, X., Nogués, M. V., de Llorens, R. & Cuchillo, C. M. (1991). *Essays Biochem.* **26**, 89–103.

Ribó, M., Beintema, J. J., Osset, M., Fernández, E., Bravo, J., de Llorens, R. & Cuchillo, C. M. (1994). *Biol. Chem. Hoppe-Seyler*, **375**, 357–363.

Richards, F. M. & Wyckoff, H. W. (1971). *The Enzymes*, 3rd ed., edited by P. D. Boyer, Vol. IV, pp. 647–806. New York: Academic Press.

Rosenberg, H. F. (1998). *Cell. Mol. Life Sci.* **54**, 811–824.

Rosenberg, H. F. & Dyer, K. D. (1996). *Nucleic Acids Res.* **24**, 3507–3513.

Roussel, A. & Cambillau, C. (1989). *Silicon Graphics Geometry Partners Directory*, pp. 77–79. Mountain View, CA, USA: Silicon Graphics.

Rybak, S. M. & Newton, D. L. (1999). *Exp. Cell Res.* **253**, 325–335.

Sasso, M. P., Lombardi, M., Confalone, E., Carsana, A., Palmieri, M. & Furia, A. (1999). *Gene*, **227**, 205–212.

Schein, C. H. (1997). *Nature Biotechnol.* **17**, 529–536.

Sorrentino, S. & Libonati, M. (1997). *FEBS Lett.* **404**, 1–5.

Strydom, D. J. (1998). *Cell. Mol. Life Sci.* **54**, 811–824.

Strydom, D. J., Fett, J. W., Lobb, R. R., Alderman, E. M., Bethune, J. L., Riordan, J. F. & Vallee, B. L. (1985). *Biochemistry*, **24**, 5486–5494.

Terzyan, S. S., Peracaula, R., de Llorens, R., Tsushima, Y., Yamada, H., Seno, M., Gomis-Rüth, F. X. & Coll, M. (1999). *J. Mol. Biol.* **285**, 205–214.

Watanabe, Y., Ueda, M., Psarras, K., Ikeda, T., Enomoto, K., Kitajima, M., Futami, J. & Seno, M. (1999). *Proc. Am. Assoc. Cancer Res.* **40**, No. 151.

Wlodawer, A., Svensson, L. A., Sjolin, L. & Gilliland, G. L. (1988). *Biochemistry*, **27**, 2705–2717.

Yamashita, K., Hitoi, A., Irie, M. & Kobata, A. (1986). *Arch. Biochem. Biophys.* **250**, 263–266.

Youle, R. J. & D'Alessio, G. (1997). In *Ribonucleases: Structures and Functions*, edited by G. D'Alessio & J. F. Riordan. New York: Academic Press.

Zegers, I., Maes, D., Dao-Thi, M.-H., Poortmans, F., Palmer, R. & Wyns, L. (1994). *Protein Sci.* **3**, 2322–2339.